Lab on a Chip
Miniaturisation for chemistry, physics, biology, & bioengineering
www.rsc.org/loc Volume 9 | 2009 |

PAPER

# High Speed Nanofluidic Protein Accumulator

**Dapeng Wu and Andrew J. Steckl**

***Nanoelectronics Lab, University of Cincinnati, Cincinnati, OH***

*Lab Chip*, **Advance Article** • DOI: 10.1039/B823409D • Publication Date (Web): 27 March 2009

*A nanoporous membrane integrated microfluidic device for million-fold protein accumulation in 200 seconds is presented.*

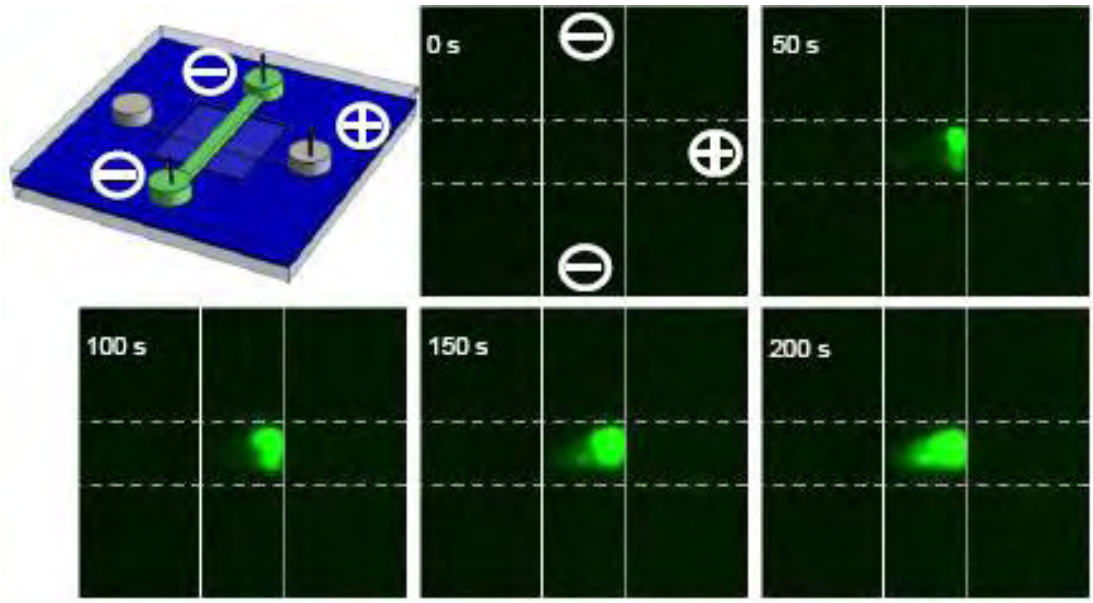

# High speed nanofluidic protein accumulator†

**Dapeng Wu and Andrew J. Steckl***

***Received 7th January 2009, Accepted 24th March 2009***
***First published as an Advance Article on the web 27th March 2009***
**DOI: 10.1039/b823409d**

Highly efficient preconcentration is a crucial prerequisite to the identification of important protein biomarkers with extremely low abundance in target biofluids. In this work, poly(dimethylsiloxane) microchips integrated with 10 nm polycarbonate nanopore membranes were utilized as high-speed protein accumulators. Double-sided injection control of electrokinetic fluid flow in the sample channel resulted in highly localized protein accumulation at a very sharp point in the channel cross point. This greatly enhanced the ability to detect very low levels of initial protein concentration. Fluorescein labeled human serum albumin solutions of 30 and 300 pM accumulated to 3 and 30 μM in only 100 s. Initial solutions as low as 0.3 and 3 pM could be concentrated within 200 s to 0.3 and 3 μM, respectively. This demonstrates a $\sim 10^5$–$10^6$ accumulation factor, and an accumulation rate as high as 5000/sec, yielding a >10× improvement over most results reported to date.

## Introduction

Biological sample preparation is of great significance for protein identification. For most commonly used diagnostic methods, such as immunoassay and liquid chromatography-mass spectrometry (LC-MS), it is still very challenging to detect target proteins with pico- to femto-molar levels. Moreover, it is critical to minimize the clinical sample amount to insure that the donor/patient health is not compromised. Common lab-top nanofiltration can only achieve hundred-fold enrichment using high-speed cooling centrifuges, and requires ~1 ml samples. Therefore, it is very important to develop techniques that maximize the quality and utility of bio-specimens for molecular analysis of clinical samples.[1]

Microfluidics is an excellent tool for biopolymer manipulation.[2] It only consumes micro- to nano-liter samples, provides superior fluid control, good compatibility with biological samples (such as on-chip cell and tissue cultures).[3] Microfluidics-based integrated biochemical analysis includes DNA extraction and amplification,[4] electrophoresis separation,[5] and molecular immunoassay.[1]

Microfluidic-based methods are also highly promising for protein enrichment. The primary traditional methods have been solid phase extraction (SPE)[6] and electrophoretic mobility gradient induced concentration (EMGIC).[7] SPE is one type of surface affinity, usually driven by pressure. SPE is a convenient preconcentration approach to couple with a micro-LC system. However, the solid phase fabrication and modification procedures in SPE are complicated and time-consuming, and they become even more so in microchannels because of space limitations. EMGIC is electrically driven and operates based on differences in buffer concentration, conductance or pH, such as isotachophoresis (ITP) and isoelectric focusing (IEF). EMGIC is compatible with microchip electrophoresis process. In EMGIC, careful tuning of buffer parameters is necessary. To date, enrichment of a few thousand-fold has been most commonly reported,[7] which is not sufficient for detection of super-low protein targets.

With the development of MEMS, nanopores can be incorporated in microdevices as required.[8] When the effective nanopore size is smaller than the effective size of protein molecules, the proteins driven by an electric field will be separated and concentrated based on the size exclusion effect.[7] Various nanofilter materials and fabrication approaches have been tested, such as crosslinked polymer plug[9] and hydrogel,[10] silica gel,[11] Nafion® film,[12] PDMS[13] and polyethylene terephthalate (PET)[14] breakdown nanogap, and PDMS/glass interface.[15] Membranes with larger (> 40 nm) nanopores have also been used,[16–19] serving as concentration polarization units to concentrate proteins. These nanofilters operate based on the dynamic balance between the bulk electro-osmotic flow (EOF) and the molecule electrophoretic mobility.[19,20] Usually, in-situ nanofilter generation is time consuming and access to special instruments is needed, both of which will increase the chip cost significantly. Most importantly, several dozens of minutes and even hours are needed for a significant concentration effect. For example, million-fold protein enrichment over a period of ~1 hour has been reported[16] with a nanofluidic filter. This is much longer than for other microfluidic approaches, where only a few (1–2) minutes are needed for chip protein electrophoresis or chromatography.

In this work, polycarbonate track etched (PCTE) nanopore membranes sandwiched in PDMS microdevices were utilized as highly efficient protein nanofilters. PCTE membranes are commercially available, with a narrow nanopore diameter distribution (< 20%), and wide diameter range from 10 nm to 30 μm. These membranes have superior mechanical strength and are relatively thin (~6–10 μm). As the membrane is integrated in the PDMS microfluidic chip, the nanopores are accessible by molecular diffusion and electric field controlled flow. PCTE

*Nanoelectronics Lab, University of Cincinnati, Cincinnati, Ohio, 45221-0030, USA. E-mail: a.steckl@uc.edu; Fax: +1 513-556-7326; Tel: +1 513-556-4777*

† Electronic supplementary information (ESI) available: Videos of 300 pM, 30 pM, 3 pM and 300 fM protein accumulation. See DOI: 10.1039/b823409d

 

membranes have been previously used as electrically actuated valves,[21,22] and for flow control allowing diffusion and prohibiting convection across the interface.[23] In this work, high-speed protein accumulation was obtained using a combination of optimized PDMS/PCTE nanopore membrane bonding and stabilization of electrokinetic fluid flow in the microdevice.

## Experimental

### Materials and device fabrication

PCTE (polycarbonate) membrane filters (47 mm diameter, polyvinylpyrrolidone coated) were obtained from Osmonics (Minnetonka, MN). Fluorescein isothiocyanate labeled human serum albumin (FITC-HSA), polysorbate surfactant Tween-20, and ethylenediaminetetraacetic acid (EDTA) were obtained from Sigma-Aldrich (St. Louis, MO), and tris(hydroxymethyl)-aminomethane (Tris), boric acid, NaOH, $H_3PO_4$ were obtained from Fisher. All of these materials were used as received, and all aqueous solutions were prepared with deionized water.

PDMS chip fabrication followed previously reported methods.[21] SU-8 2010 photoresist (Microchem, Newton, MA) was spun on a silicon wafer at 2000 rpm for 100 s. After 15 min soft bake at 65 °C, the SU-8 film was exposed on an EVG420 Mask Aligner (Electronics Visions, Phoenix, AZ). This was followed by 15 min 95 °C post baking, development for 3 min in propylene glycol methyl ether acetate (PGMEA) (MicroChem), and finally hard baking at 180 °C for 1 hour. The SU-8 master pattern was 15 μm deep and 50 μm wide. Sylgard 184 PDMS prepolymer mixture (10:1) was cast on the master. After curing at 80 °C for 2 hours, the PDMS layer was peeled off, reservoir holes were punched, and top and bottom PDMS components were ready for chip integration (Fig. 1).

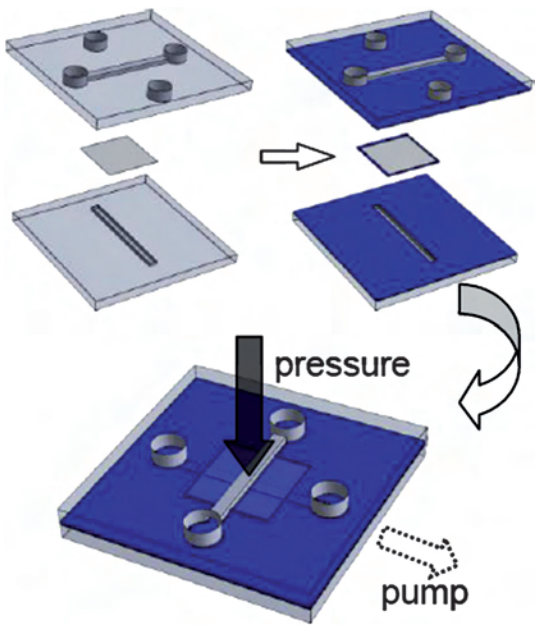


**Fig. 1** Schematic drawing of PDMS/nanopore membrane fabrication process. PDMS chips were a 3 mm-thick and 20 mm-long square, in which the channel was of 15 μm deep and 50 μm wide. PDMS chips were stamp coated with 3 μm thick PDMS glue (blue), and PCTE membrane boundaries were also dip coated in the PDMS glue. PDMS chips were joined together with channels crossed in the middle point and membrane sandwiched in the center, and the PDMS glue was fully cured in a vacuum oven with a pressure applied on the chip.

The PCTE nanoporous membrane was bonded in the PDMS chip using previously reported methods.[23,24] PDMS prepolymer liquid was used as the bonding glue, and procedures were optimized as needed. PDMS prepolymer was mixed with hexane in 1:3 ratio, and spun on plain Gold Seal Micro Slides at 2000 rpm for 30 s. After the evaporation of hexane for 10 min, a ~3 μm thick PDMS glue film was formed. PDMS microchips were stamped on the glue for 2 min. A 4 × 4 mm PCTE membrane was cut, and membrane boundaries were dip coated on the PDMS glue. Finally, this membrane was sandwiched between the upper and lower PDMS components to form the integrated microchip. The assembled device was placed horizontally in an oven, and vacuum pumped for 30 min, then a 1 kg weight was placed on the chip for 12 hours on 80 °C.

### EOF and electrophoretic mobility measurements

The current monitoring method was used to measure EOF mobility in the PDMS microchannel ($\mu_{EOF}$).[25] High conductivity buffer, 100 mM tris-borate EDTA (TBE) or 10 mM phosphate buffer, with 0.4% Tween-20 was filled into a 3.7 cm long sample channel ($L$) and one of the end reservoirs. The opposite reservoir was filled with a low conductivity buffer, a 1:2 diluted TBE or phosphate solution. Under an applied voltage of 800 V, the current decreased with time as the low conductivity buffer gradually filled the channel. The EOF mobility is obtained as

$$\mu_{EOF} = L^2/(V \cdot t_f) \quad (1)$$

where $t_f$ is the time for travel between the reservoirs to be completed. A similar method was used to detect the FITC-HSA electrophoretic mobility ($\mu_{eph}$). One reservoir and the channel were filled with buffer, while the second reservoir was filled with a buffer solution containing 0.1 mg/ml FITC-HSA. Under the same voltage of 800 V, the time ($t_{flu}$) for protein travel between the reservoir and the detection point ($L_{det}$ = 3.5 cm) was monitored by fluorescence. The apparent electrophoretic mobility can then be calculated as

$$\mu_{eph} = L \cdot L_{det}/(V \cdot t_{flu}) \quad (2)$$

### Electrokinetic protein accumulation

TBE (100 mM, pH 8.3) and phosphate (10 mM, pH 8.3) buffers were used in this work. Test samples were prepared daily from 2 mg/ml FITC-HSA stock solution, to avoid protein loss due to the surface adsorption on plastic tubes.

First, the microchannel was flushed with 1% Tween-20 water solution to convert the hydrophobic PDMS surface into a hydrophilic surface, and facilitate solution filling. Flushing with 1% Tween-20 water solution was repeated between experiments, in order to remove protein residues adsorbed on surface, and to regenerate the hydrophilic surface coating. The residual

fluorescence was also bleached for 4 min with a 25 mW 355 nm He-Cd laser (Omnichrome Corp., CA).

A high voltage unit (VITREK, 944i Dielectric Analyzer) (Fortronic Corp., Melrose, MA) was used with a maximum 10 mA, 1 kV DC output with 100 V steps. A fluorescence microscope (Labophot-2, Nikon) coupled with Moticam 5000 cooled CCD camera (Causeway Bay, HK) was used to monitor fluid flow within the microchannels. Videos and images were captured with Motic Images Advanced 3.2 software (Causeway Bay, HK) with a 2000 gain, 0.2 s exposure time, and 5 s interval time between two video pictures. Fluorescent intensity was analyzed with Image J (free software).

## Results and discussion

### Vacuum- and pressure-assisted chip bonding

The PDMS/membrane binding plays a crucial role in determining the accumulation efficiency. Since nanogaps frequently occur in two-layer microdevices bonded based on PDMS surface hydrophobicity or sandwiched between oxygen plasma treated PDMS chips, obvious liquid leakage can take place along membrane boundaries *via* capillary force. We have used PDMS glue to improve the sealing of the membrane to the PDMS layers, which has been reported to significantly alleviate liquid leakage.[23,24] However, we have found that air bubbles were still present along membrane boundaries, especially around the PDMS channel, as the PCTE membrane is ~10 μm thick and its boundary is fairly rough due to cutting. Increasing the PDMS glue layer thickness from 3 to 6 μm to prevent air bubbles frequently resulted in a blocked channel due to PDMS glue infiltration.

A more effective method for chip/membrane bonding was realized using a combination of a pressure (on the chip) and vacuum (in the channel). As the PDMS glue was being cured, pressure on the chip reduces the gap due to the PDMS flexible transformation and at the same time increases the flow of PDMS glue into the gap around the membrane boundary and the PDMS/membrane interface. After curing, no air bubbles were present, and fluid leakage in the device was inhibited. More importantly, no fluid leakage occurred during high voltage operation. During operation at a voltage as high as 1 kV, proteins were localized within the cross zone of the chip. Perfect PDMS/membrane bonding is very important for high efficiency protein accumulation, since expansion of the focused protein location and leakage into the bottom channel *via* membrane boundary decreases the signal strength and leads to non-reproducible accumulation results (Fig. 2).

### Stabilized fluidic flow in the microchannel

In our experiments, when 0.4% Tween-20 (neutral surfactant) was added in the TBE buffer, the EOF in the microchannel was inhibited, resulting in a very low $\mu_{EOF} = 7.6 \times 10^{-5}$ cm$^2$/(V s). The movement of FITC-HSA was dominated by its electrophoretic mobility. The membrane blocked the transfer of FITC-HSA between sample and buffer channels and therefore it accumulated on the membrane. In most nanofilter microdevices, the nanopore diameter is typically less than 10 nm. These include silica gel,[11,26] Nafion® film,[12,27,28] native nanogap between PDMS and glass,[15] breakdown nanogap in PDMS and PET microdevices,[13,14] and the 25% crosslinked polyacrylamide hydrogel.[10,29] In this work, nanopore membranes with 10 nm pores were used. The pore diameter is larger than the nominal size of FITC-HSA molecules, which is approximately $8 \times 8 \times 3$ nm$^3$. Therefore, protein molecules should, in principle, be transported through the membrane when a high electric field is applied. In fact, no FITC-HSA transport through the membrane was observed. This suggests that the inner surfaces of PCTE nanopores were negatively charged.[30] This is probably due to the fact PVP did not completely coat the nanopore, although PVP had thoroughly covered the

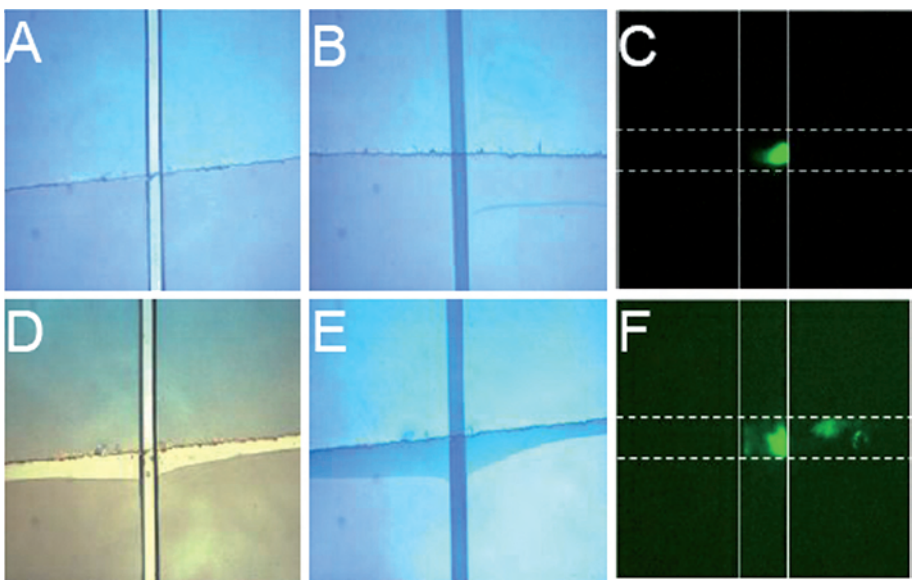


**Fig. 2** Comparison of PDMS glue bonded PDMS/nanopore membrane microdevice with and without vacuum and pressure assistance. Device bonded with vacuum and pressure assistance (A), filled with solution (B), and electrokinetic accumulation with 1000 V voltage added (C). Device bonded without vacuum and pressure assistance (D), filled with solution (E), and electrokinetic accumulation with 1000 V voltage added (F).

membrane surface and rendered it hydrophilic. The electrical double layer (EDL) in the small nanopore should overlap and increase the related ion selectivity against negatively charged FITC-HSA molecules.[30,31] Under 100 mM TBE solution, the EDL thickness is in the range of 3 $\sim$ 4 nm,[32] so the effective free nanopore diameter is < 4 nm. While the small FITC molecules could be transported freely, the larger FITC-HSA molecules were blocked. It has been reported that membranes with 15 nm nanopore had a cut-off molecular weight of 10 kDa for dextran molecules in 5 mM phosphate buffer,[21] and 10 nm nanopores could be used to block 411 bp dsDNA in TBE buffer.[33]

Single-sided injection (SSI) and double-sided injection (DSI) were tested with TBE buffer. It was found the fluid flow using SSI was unstable in most cases, with the focused proteins departing from the cross-channel zone and flowing into either side of the sample channel. Possible factors causing this unstable flow include: (1) Laplace pressure from sample liquid curvature difference between the two end reservoirs, which would dominate hydrodynamic flow in the microchannel;[34,35] (2) EOF from nanopores; as discussed above, nanopores are negatively charged, and should have a positive EOF,[36] which will push the sample flow away from the cross point; (3) concentration polarization,[20] which will induce molecular diffusion. Using DSI, the very high pinched electric field which develops at the cross-point could withstand hydrostatic flow and molecular diffusion, and balance the EOF from nanopores into the two sides of sample channel (Fig. 3).

We have also investigated the effect of different buffer solutions on protein accumulation. When 10 mM phosphate buffer was used instead of 100 mM TBE buffer, protein accumulation completely disappeared. In the first 30 s, protein was found to move to the cross-point area, but no obvious focusing point could be defined, and all protein scattered in the center of the sample channel. After that, the centered sample was pushed away from the cross point into the two sides of the channel. At the end of 200 s, nearly no protein was found near the cross-point.

To determine the mechanisms leading to different fluid flow behavior in the two buffer solutions, the FITC-HSA electrophoretic mobility ($\mu_{eph}$) and the bulk flow EOF mobility ($\mu_{EOF}$) in the microchannel were measured. $\mu_{EOF}$ was $(6.9 \pm 0.7) \times 10^{-5}$ cm$^2$/(V s) and $(7.6 \pm 1) \times 10^{-5}$ cm$^2$/(V s), and $\mu_{eph}$ was $(2.9 \pm 0.3) \times 10^{-4}$ cm$^2$/(V s) and $(2.7 \pm 0.2) \times 10^{-4}$ cm$^2$/(V s) for phosphate and TBE buffers, respectively. Since no significant differences were found between EOF mobilities in the phosphate and TBE buffers, electrokinetic movement in the microchannel was not the dominant factor in determining fluid flow behavior. Therefore, it is likely that the change of nanopore EOF is responsible for the failed protein accumulation in phosphate buffer. Higher Joule heating (due to a current of $\sim$30 μA vs. $\sim$15 μA in TBE buffer) is suggested as the cause of EOF change. Joule heating leads to an increase in liquid temperature, which in turn leads to decreased liquid viscosity and to increased ionized nanopore surface chemical groups. The combination of decreased viscosity and increased ionized surface results in a sharp increase of nanopore EOF. Eventually, the nanopore EOF exceeds the EOF in the microchannel. At that point the pressure induced flow is greater than the electrophoretic mobility of FITC-HSA in the microchannel but in opposite direction, thus forcing protein molecules away from the cross-point area. Therefore, 100 mM TBE buffer and DSI were used in the following protein accumulation experiments.

### High-speed protein accumulation

For FITC-HSA samples of initial concentration ranging from 300 fM to 300 pM, electrokinetic injection and accumulation was performed for $\sim$200–400 s with TBE buffer and DSI. The fluorescence signal was averaged over a 5 μm × 5 μm area in the

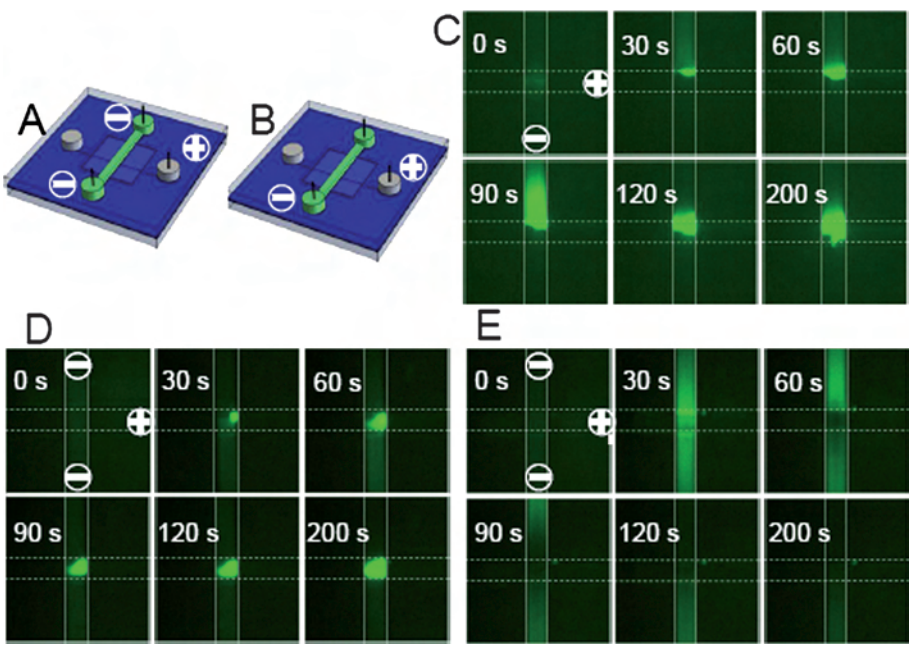


**Fig. 3** The effect of buffers and injection modes to electrokinetic flow in the microchannel. Double side injection (DSI) (A), single side injection (SSI) (B), TBE buffer and SSI injection (C), TBE buffer and DSI injection (D), and phosphorate buffer and DSI injection (E).

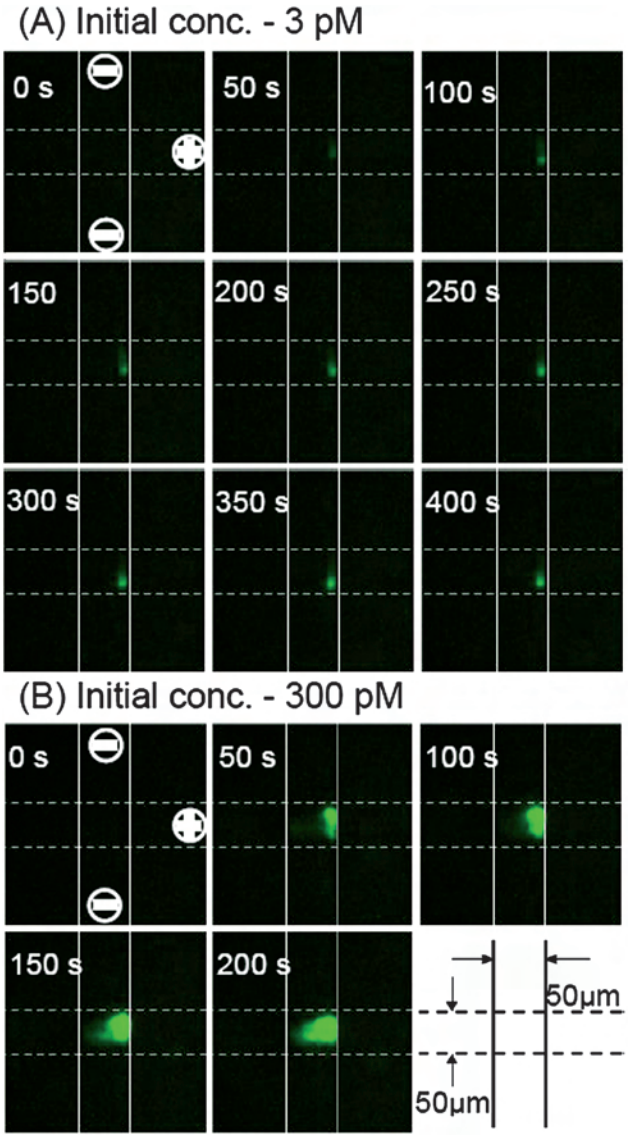


**Fig. 4** Images of 3 pM FITC-HSA accumulation with time on the membrane to the vicinity of the cross channel zone (A). Images of 300 pM FITC-HSA accumulation with time on the membrane around the cross channel zone (B).The cross-point has an area of 50 × 50 μm$^2$.

region of strongest intensity (Fig. 4). The signals increased very quickly, reaching the intensities associated with concentrations of 0.3 μM and 3 μM for an accumulation gain of $10^6$ within ~200 s. Most proteins were accumulated on a very small region of the overall cross-point area (2500 μm$^2$).

The change of fluorescence intensity with time provides a measure of the protein accumulation rate ($\alpha_{fl}$) and can be used as a figure of merit by which one can compare the efficiency of different techniques:

$$\alpha_{fl} = G/t_{acc} = (C_f/C_i)/t_{acc} \quad (3)$$

where $G$ is the accumulation gain given by the ratio of the final ($C_f$) and initial ($C_i$) concentrations, and $t_{acc}$ is the accumulation time. The measured values of $\alpha_{fl}$ ranged from 1,000 s$^{-1}$ to 9,000 s$^{-1}$, depending on the initial concentration.

The accumulation rate can also be calculated from the apparent electrophoretic mobility ($\mu_{eph}$):

$$\alpha_{eph} = 2\mu_{eph} \cdot E_{ch} \cdot W_{ch}/A_{pro} \quad (4)$$

where $E_{ch}$ is the electric field in the sample channel, $W_{ch}$ is the channel width, $A_{pro}$ is the area of protein accumulation, and the factor of 2 accounts for the dual injection mode. By measuring the current flow in the channel with and without membrane separation, resistances of ~40 and ~10 MΩ were obtained for the channel and the membrane, respectively. For an applied bias of 800 V, this translates into an electric field in the channel during protein accumulation of ~450 V/cm. For a typical accumulation region of 5 × 5 μm$^2$, a value of $\alpha_{eph}$ of ~4,900 s$^{-1}$ is calculated, while for an area of 5 × 10 μm$^2$ a corresponding value of ~2,450 s$^{-1}$ is obtained. The calculated $\alpha_{eph}$ accumulation rate values agree quite well with the range of experimentally measured $\alpha_{fl}$ values. This indicates that the 10 nm nanopore membrane completely blocks FITC-HSA transport. If the protein molecules were collected over the entire channel cross area (50 μm × 50 μm), then $\alpha_{eph}$ would be only 58 s$^{-1}$. Therefore, a sharply focused protein accumulation region is a key factor for achieving a high speed concentration effect. The results reported here represent a significant improvement on earlier pioneering efforts. For example, the first report[21] on using a PCTE membrane as an electrically activated valve showed that large molecules (2 MDa FITC-labeled dextran) were blocked by 15 nm pores. However, no attempt at using this effect to obtain enrichment was reported. Another report[33] on using 10 nm PCTE membranes for pre-concentration of 411 bp DNA molecules yielded enrichment of 80× and an accumulation rate of 2 s$^{-1}$.

It is interesting to note that protein molecules accumulated preferentially to the anode side of the PDMS/membrane boundary. Similar phenomenon had been observed in protein concentration with in-situ fabricated polymer plug.[9] This is probably caused by the electric field gradient on the membrane surface. Moreover, the accumulation started as a sharp point usually close to the entry point of one of the side channels, rather than uniformly along the entire boundary line. The non-homogeneous membrane thickness and nanopore diameter variation are probably the main reasons for this effect. Proteins should accumulate first in the membrane region of lower thickness (and therefore lower voltage drop) and with larger nanopores.

As shown in Fig. 4, for the highest initial protein concentration of 300 pM, the focused area expanded when the focused protein concentration exceeded 30 μM after 100 s. This probably was caused by molecular diffusion due to such a high concentration. Therefore, in this case, the fluorescence intensity did not increase as fast as those at lower initial protein concentration, resulting in $10^5$ concentration gain in ~80 s (Fig. 5). This corresponds to an accumulation rate of ~1.25 × $10^3$ s$^{-1}$. The samples with lower initial concentrations (300 fM and 3 pM) experienced higher accumulation rates of ~6 × $10^3$ s$^{-1}$ and 9 × $10^3$ s$^{-1}$, respectively. This resulted in concentration gains of $10^6$ within 2–3 min.

## Summary and conclusion

In this work, high speed protein concentration in ~200 s was demonstrated successfully. Vacuum and pressure-assisted

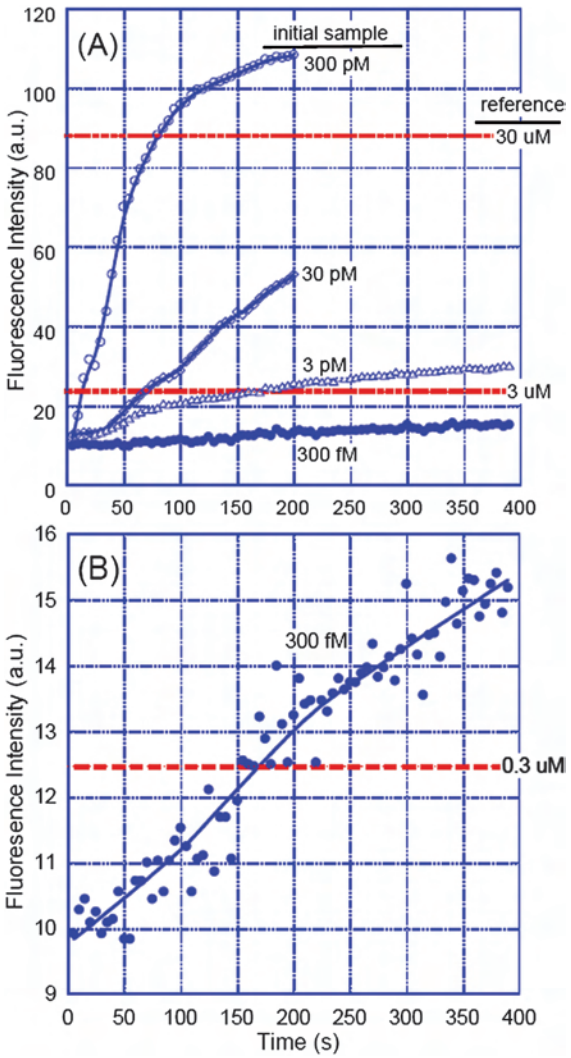


**Fig. 5** Electrokinetic accumulation of FITC-HSA with different initial concentrations. The curves of fluorescence intensity with time from 300 pM, 30 pM, 3 pM and 300 fM individually (A). Close-up view of 300 fM FITC-HSA accumulation about fluorescence intensity with time (B).

PDMS/nanopore membrane bonding with PDMS glue was shown to completely inhibit residual air bubbles along PDMS boundaries, and to prevent leakage into the nanogap between the membrane and the PDMS layers. Therefore, all protein molecules were accumulated within the cross channel area. Double-sided sample injection in TBE buffer with 0.4% Tween-20 addition effectively stabilized the fluid flow in the microchannel, resulting in stable protein accumulation into the cross-channel zone. The electrical field gradient on the cross-channel membrane produced a sharp point effect which induced protein accumulation in a very small zone. Using a high electric field (800 V/cm), a $10^5$ to $10^6$-fold increase in concentration of FITC-HSA could be achieved in less than 200 s, yielding an accumulation rate of ~5,000–10,000 $s^{-1}$.

If laser excitation is used instead of a mercury lamp in the fluorescence microscopy, the detection limit hopefully can be further improved ~$10^3$ fold, which will lead to identification of protein samples of fM to aM concentration after only a short enrichment time (a few seconds). Coupled with mass spectrometry, this microdevice has the potential to greatly broaden the detection range. In real world applications, target proteins exist in a complex biological mixture with highly abundant background impurities. Selective protein capture coupled with the very efficient enrichment approach presented here will have wide applicability.

## Acknowledgements

This work was partially supported by grants from DARPA (#USAF FA8650-07-C-7717) and NSF (ECCS-0725530).

## References

1 P. Yager, T. Edwards, E. Fu, K. Helton, K. Nelson, M. R. Tam and B. H. Weigl, *Nature*, 2006, **442**, 412–418.
2 G. M. Whitesides, *Nature*, 2006, **442**, 368–373.
3 F. K. Balagadde, L. C. You, C. L. Hansen, F. H. Arnold and S. R. Quake, *Science*, 2005, **309**, 137–140.
4 C. J. Easley, J. M. Karlinsey, J. M. Bienvenue, L. A. Legendre, M. G. Roper, S. H. Feldman, M. A. Hughes, E. L. Hewlett, T. J. Merkel, J. P. Ferrance and J. P. Landers, *Proc. Natl. Acad. Sci. USA*, 2006, **103**, 19272–19277.
5 D. P. Wu, J. H. Qin and B. C. Lin, *J. Chromatogr., A*, 2008, **1184**, 542–559.
6 M. H. Fortier, E. Bonneil, P. Goodley and P. Thibault, *Anal. Chem.*, 2005, **77**, 1631–1640.
7 J. Y. Han, J. P. Fu and R. B. Schoch, *Lab Chip*, 2008, **8**, 23–33.
8 J. Han and H. G. Craighead, *Science*, 2000, **288**, 1026–1029.
9 S. Song, A. K. Singh and B. J. Kirby, *Anal. Chem.*, 2004, **76**, 4589–4592.
10 A. V. Hatch, A. E. Herr, D. J. Throckmorton, J. S. Brennan and A. K. Singh, *Anal. Chem.*, 2006, **78**, 4976–4984.
11 R. S. Foote, J. Khandurina, S. C. Jacobson and J. M. Ramsey, *Anal. Chem.*, 2005, **77**, 57–63.
12 S. J. Kim and J. Y. Han, *Anal. Chem.*, 2008, **80**, 3507–3511.
13 J. H. Lee, S. Chung, S. J. Kim and J. Y. Han, *Anal. Chem.*, 2007, **79**, 6868–6873.
14 H. Yu, Y. Lu, Y. G. Zhou, F. B. Wang, F. Y. He and X. H. Xia, *Lab Chip*, 2008, **8**, 1496–1501.
15 S. M. Kim, M. A. Burns and E. F. Hasselbrink, *Anal. Chem.*, 2006, **78**, 4779–4785.
16 Y. C. Wang, A. L. Stevens and J. Y. Han, *Anal. Chem.*, 2005, **77**, 4293–4299.
17 J. H. Dai, T. Ito, L. Sun and R. M. Crooks, *J. Am. Chem. Soc.*, 2003, **125**, 13026–13027.
18 R. Dhopeshwarkar, D. Hlushkou, M. Nguyen, U. Tallarek and R. M. Crooks, *J. Am. Chem. Soc.*, 2008, **130**, 10480–10481.
19 Y. Zhang and A. T. Timperman, *Analyst*, 2003, **128**, 537–542.
20 S. J. Kim, Y. C. Wang, J. H. Lee, H. Jang and J. Han, *Phys. Rev. Lett.*, 2007, **99**.
21 T. C. Kuo, D. M. Cannon, Y. N. Chen, J. J. Tulock, M. A. Shannon, J. V. Sweedler and P. W. Bohn, *Anal. Chem.*, 2003, **75**, 1861–1867.
22 K. Fa, J. J. Tulock, J. V. Sweedler and P. W. Bohn, *J. Am. Chem. Soc.*, 2005, **127**, 13928–13933.
23 R. F. Ismagilov, J. M. K. Ng, P. J. A. Kenis and G. M. Whitesides, *Anal. Chem.*, 2001, **73**, 5207–5213.
24 B. H. Chueh, D. Huh, C. R. Kyrtsos, T. Houssin, N. Futai and S. Takayama, *Anal. Chem.*, 2007, **79**, 3504–3508.
25 X. Huang, M. J. Gordon and R. N. Zare, *Anal. Chem.*, 1988, **60**, 1837–1838.
26 J. Khandurina, S. C. Jacobson, L. C. Waters, R. S. Foote and J. M. Ramsey, *Anal. Chem.*, 1999, **71**, 1815–1819.
27 J. H. Lee, Y. A. Song and J. Y. Han, *Lab Chip*, 2008, **8**, 596–601.
28 M. A. Hickner, H. Ghassemi, Y. S. Kim, B. R. Einsla and J. E. McGrath, *Chem. Rev.*, 2004, **104**, 4587–4611.
29 M. L. White and G. H. Dorion, *J. Polym. Sci., Part A: Polym. Chem.*, 1961, **55**, 731–740.
30 I. Vlassiouk, S. Smirnov and Z. Siwy, *Nano Lett.*, 2008, **8**, 1978–1985.

31 R. Karnik, R. Fan, M. Yue, D. Y. Li, P. D. Yang and A. Majumdar, *Nano Lett.*, 2005, **5**, 943–948.
32 P. J. Kemery, J. K. Steehler and P. W. Bohn, *Langmuir*, 1998, **14**, 2884–2889.
33 Z. C. Long, D. Y. Liu, N. N. Ye, J. H. Qin and B. C. Lin, *Electrophoresis*, 2006, **27**, 4927–4934.
34 H. J. Crabtree, E. C. S. Cheong, D. A. Tilroe and C. J. Backhouse, *Anal. Chem.*, 2001, **73**, 4079–4086.
35 M. J. Gong, K. R. Wehmeyer, A. M. Stalcup, P. A. Limbach and W. R. Heineman, *Electrophoresis*, 2007, **28**, 1564–1571.
36 D. Krapf, B. M. Quinn, M. Y. Wu, H. W. Zandbergen, C. Dekker and S. G. Lemay, *Nano Lett.*, 2006, **6**, 2531–2535.

 